European Journal of Science and Theology, October 2017, Vol.13, No.5, 185-206

CORROSION MECHANISM OF IRON OBJECTS IN MARINE ENVIRONMENT AN ANALYTICAL INVESTIGATION STUDY BY RAMAN SPECTROMETRY

S. Ahmed Saleh*

Fayoum University, Faculty of Archaeology, Department of Restoration and Conservation of Archaeological Material, Fayoum Governorate, 63514, Egypt

(Received 31 August 2016, revised 8 June 2017)

Abstract

Iron is one of the most recovered historical materials from the marine environment. Two iron parts from historical ships were excavated from Paros Island, Greece. Even though hard, thick and non-porous crust from the marine sediments was found on the wrought iron surfaces, the most of these objects have remained in worst conditions caused by the corrosion process in marine environment. The main purpose of the Raman investigation and analysis was a classification and characterization of the corrosion compounds and their phases and the marine sediments by assignment of phases and comparison to standard reference materials.

Microraman spectrometry is a non-destructive technique, and the error rate of analysis result is lower than other methods. The instrumental condition of Raman spectra for investigation and analysis in the 100-3500 cm^{-1} wavenumber region allowed the characterization of solid deposits of iron and external encrustation. Discrimination between corrosion compounds by Raman spectroscopy has been demonstrated. The final results of this study revealed that goethite, hematite and lepidocrocite are the major minerals and akaganeite was highly detected in the rust.

Keywords: rust, marine environment, Raman spectrometry, analysis, investigation

1. Introduction

The historical iron surfaces are modified in marine environment by deposition of corrosion products combined with seawater minerals. Therefore further corrosion occurred after extraction the iron objects from marine environmental condition resulting from exposing to a new environment that tends to transform the ductile metal into corrosion products. Few authors have studied the corrosion systems of iron artefacts removed from marine environment [1-5]. Seawater is a corrosive medium resulting from its

*E-mail: sms02@fayoum.edu.eg

composition that represents the electrolyte of corrosion process. Iron is a ubiquitous metal that is often unstable due to its chemical activation, especially in the marine environment rich in chloride ions [6].

Corrosion is the gradual physiochemical destruction of a metal through chemical or electrochemical reactions with the surrounding media beginning from its surface [7, 8]. Corrosion process produces new bonds at the surface between the metal and corrosion compounds [9] and it leads to the loss of most physical properties as mechanical strength and modifies the chemical structure. The corrosion rate depends on the composition of the iron object, the water's electrical conductivity, oxygen concentration, temperature, and acidity [10]. Pure iron acts as anode, impure surfaces acts as cathode and dissolved chloride, oxygen or carbon dioxide contribute to the corrosion rate [6].

Rusting of iron is the most important redox reaction [11]. The basic process of metallic corrosion in aqueous solution consists of the anodic dissolution of metals and the cathodic reduction of oxidants present in the saline water [12].

Oxidation is the main cause of damage to iron objects in seawater, because the electrochemistry of metal oxide [13]. The oxygen concentration of seawater varies significantly with the depth of the object, but also with the temperature and the biological activity of seawater [14].

When iron corrodes, the corrosion rate is usually controlled by the cathodic reaction, which in general is much slower [15]. Reaction involves the reduction of water, which is often facilitated by anaerobic bacteria under saline sediment [16]. Sulphate-reducing bacteria are commonly found in saltwater [17]. Magnetite, goethite and lepidocrocite are not previously known to be biological precipitates in the marine environment [18].

Corrosion mechanism in the marine environment can be described with a reaction model as follows:

$$Fe^{0}_{(s)} \rightarrow Fe^{2+}_{(aq)} + 2e^{-} \quad (1)$$

$$Fe^{2+}_{(aq)} \rightarrow Fe^{3+}_{(aq)} + e^{-} \quad (2)$$

$$H_2O + CO_{2(g)} \rightarrow H_2CO_{3(aq)} \rightarrow 2H^{+}_{(aq)} + CO_3^{2-}{}_{(aq)} \quad (3)$$

Both anodes of Fe^{2+} and Fe^{3+} migrate through water adhering to metal surface with the cathode surface. Fe^{2+} at the surface will be further oxidized by oxygen producing iron oxides [19].

$$4Fe^{2+} + O_2 + (4+x)H_2O \rightarrow 2Fe_2O_3 \cdot xH_2O(s) + 8H^{+} \quad (4)$$

At lower level of Cl^{-} ions, the corrosion rate decreases at near neutral to alkaline region of the medium. Both temperature and dissolved oxygen aggravate the corrosion rate [20]. At the same time, corrosion potential becomes more negative with increasing NaCl concentration [21].

The increased alkalinity of the solution under the marine concretion have a much smaller effect on the overall corrosion process than the reduction in the chloride ion concentration [16].

Salinity is the dissolved materials in seawater that alters from the water properties [22]. Most elements found on land are also found dissolved in seawater [23] which contains soluble salts. The main ions present in seawater are

Na^+ and Cl^-, Ca^{2+}, O^{2-} and the level of SO_4^{2-} is also high [24]. Saline water aggravates the weathering of iron objects. It leads to the removal of passive oxide (magnetite) and the increase of akaganeite [www.werf.org] resulting from migration of chlorine inside the metal. The extraction of the objects from marine environment favours abrupt changes resulting from the reactivation of many alteration processes to stabilize [25]. The ability of Cl^- ions to diffuse through a solution permeating a corrosion layer lies on the pore size, channel size, and their connectivity within the solid [26]. During sinking of iron objects, chloride is attracted to anodes as a counter ion to balance charge from Fe^{2+}. Soluble chloride acts as an electrolyte making the iron inherently unstable. Overlying the corroding metal core is a dense corrosion product layer identified as comprising goethite (α-FeOOH) or sometimes siderite ($FeCO_3$), magnetite (Fe_3O_4) or maghemite (γ-Fe_2O_3) strips. This is effectively the marker layer for the surface of the object and it also exists in totally mineralized objects [27].

Chloride helps in breaking passive oxide layers, leading to localized corrosion [28] that is found usually in pits and crevices [29] due to the deep penetration and electronegativity of chloride ions [30]. So pitting corrosion is an important form of localized corrosion.

The erosion corrosion is the attack of a metal caused by the rapid flow of a fluid past or the impingement of a fluid on the metal surface. Steels and iron alloys are most subject to this form of attack in seawater [28, 31].

New technology introduces other methods for identification of the corrosion products, coupled with the wide range of instrumental and sampling methodologies available. Raman spectroscopy is an easy, and non-destructive, inexpensive screening system [32] that is sometimes more powerful than X-ray analysis for detecting and monitoring crystallisation/amorphisation or organic and inorganic materials [31], and it is able to distinguish between mineral polymorphs [33] with high accuracy and low error rate [34].

Raman scattering has been introduced as a vibrational spectroscopy technique complementary to infrared spectroscopy for chemical analysis [35]. Laser Raman spectroscopy is an optical technique in which a laser excites a target and the spectrum of the energy-shifted, back-scattered radiation serves as a fingerprint, providing compositional and structural information. Raman spectroscopy has been performed to analyse minerals since its discovery in 1928 [33].

At the same time, there were attempts to characterize the inorganic materials as corrosion products [36] and detecting degradation products of archaeological materials [35]. On November 2001, Raman spectroscopy was hosted by The British museum and generated considerable enthusiasm [37]. It's sufficient to use a few milligrams from the sample. Small artefacts can be investigated and analysed without taking any sample. It is possible to get Raman spectra for crystals, powders, polymers and coloured solutions [38].

Raman spectroscopy has been found to be very sensitive to the physicochemical state of the metal oxide, with Raman frequencies being dependent on the metallic oxidation state [39]. Nowdays, Raman detectors, or

Charge Coupled Device detectors (CCDs) have a wide dynamic range and users can select the appropriate exposure time for their sample [www.perkinelmer.com]. Raman spectroscopy provides detailed insight on the electronic structure for complexes with an intense absorption band at the excitation wavelength used. The electromagnetic radiation, colliding with a molecule, can be transmitted, observed, or scattered. When the collision is elastic, the incident and the scattered radiation have the same frequency. On the contrary, in an inelastic collision, the scattered radiation has either higher or lower frequency with respect to the incident one, giving the so-called Raman scattering [40].

Laser is used in Raman spectrometry because it gives high intensity and the light can easily be focused in a small area (1μm) of the sample. Laser is also polarized and this can be used to identify the depolarization ratio.

The light source of a Raman spectrometer must give intense radiation for the scattered light to be strong enough for observation. In addition, the light should be monochromatic [41]. The scattering intensity varies by orders of magnitude depending on the bond polarizability (the more covalent the bonds, the higher the number of electrons involved and the higher the Raman peak intensity), the crystal symmetry and the exciting wavelength [31, 42].

Whenever the absorbing phase is not dispersed in a transparent matrix, a significant part of the scattered light intensity may be reabsorbed [43].

The primary concern of this work is to investigate and analyse two marine objects by Raman spectroscopy for determination the marine corrosion products and the marine deposits. Study of corrosion mechanism in marine environment is very important to assess the conservation and preservation plan.

2. Condition of the iron objects

Some historical iron objects were leached from the marine environment at Paros Island in Greece. These objects represent the top of unknown historical ship, and they are free of decorative units.

Iron objects were found in poor condition resulting from deterioration occurring during long-term submergence. Objects lying proud of the seabed had higher corrosion potentials than other objects at the same depth which were more buried in the surrounding reef platform [44]. Non-metallic materials closed with iron objects playing a physical adsorption that represent a continuous source of electrolytes after removing from water.

Some historical iron objects were carefully removed from the original environment by divers that have been found after excavations covering with hard, thick and non-porous and saturated with chloride ions (Figure 1). Concreted layer made up calcium carbonate, gypsum, orthoclase, quartz, algae, and marine plants.

As shown in Figure 2a that sketches the mechanism of corrosion process of iron objects in seawater, the major elements playing the most effect in activation of corrosion process in seawater are sodium, chlorine, magnesium,

sulphur, and calcium. The presence of these ions control corrosion process in seawater. After long sinking of iron objects in seawater, two basic layers were built up as a corresponding cathodic reaction of the corrosion process (Figure 2b).

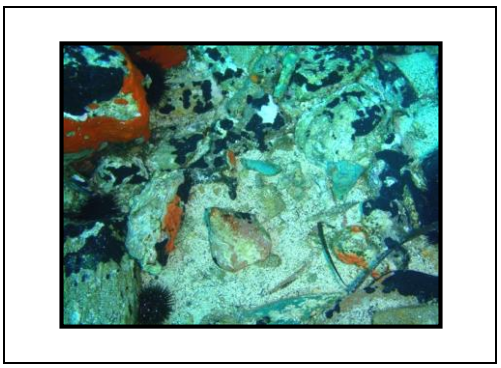

Figure 1. The as-found condition of iron objects in the original environment of the marine objects at Paros Island.

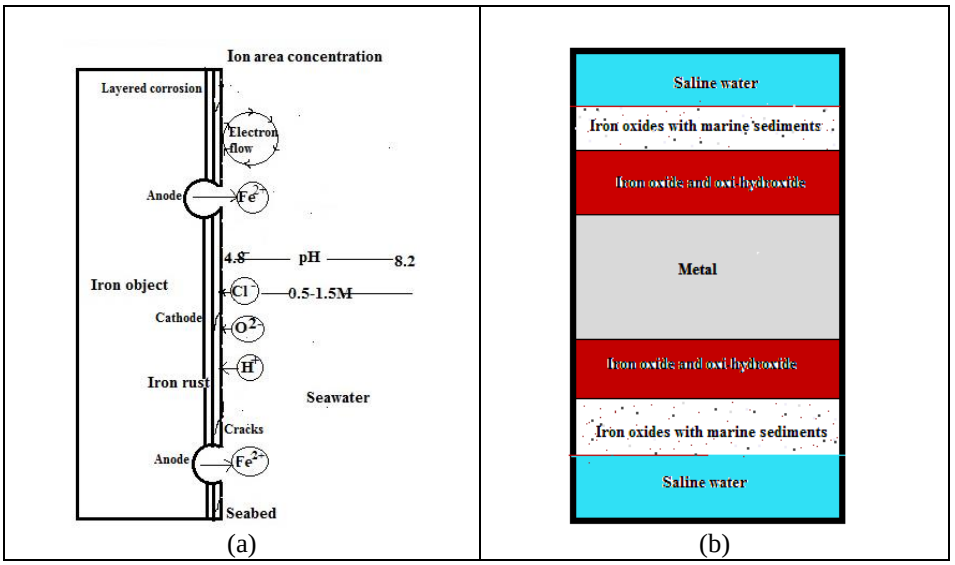

Figure 2. (a) Mechanism of corrosion process of iron object in seawater, (b) Cross schematic of corrosion products in seawater.

Even though the deposits that appear on the iron surface are thick, nonporous and compact, they did not prevent the activation of corrosion process, and most of the metallic iron was transformed into corrosion compounds. The corrosion activity took place and continued in the most parts of the iron objects. Marine wrought iron looks like old wood or fibrous structure. After removing the marine encrustations, the surface morphology of iron object is not even. Also, the dimensions of diameter of the core were changed caused by post-excavation corrosion of the iron objects. Photo-documentation of the iron objects

was performed to highlight the rate of corrosion process as shown in Figures 3-9.

It is reasonable to assume that colour, hardness, friability and inclusions are characteristic of corrosion products by visual and optical investigation.

(a) (b)

Figure 3. (a) The remains of the first iron object, (b) Loss part and cracks on the sediment layer of the iron object tended to flack off the marine concretion.

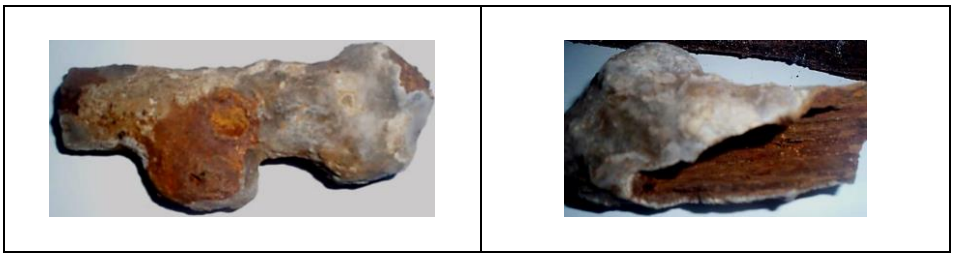

Figure 4. Surface is covered by iron oxides of the object. Some parts were loosed in the external layer caused by the mechanical effect of seawater.

(a) (b)

Figure 5. (a) Weeping aspect of marine iron object after excavation for 6 years, (b) Wrought iron object that represents the top part of historical ship.

(a) (b)

Figure 6. (a) Wrought iron object flaking off the exterior layer (marine deposits); (b) The same previous part after 5 years that blacken by exposing to atmospheric corrosion process. Chemical alteration of object colour is caused by the further oxidation and reaction of chloride ions with relative humidity (thin electrolyte).

(a)

(b)

Figure 7. (a) Holes on the external layer that represents the mean of penetration the sea elements inside the iron object; (b) The morphology of the iron object core that looks like the old wood. Also, layered corrosion is the main corrosion form in this area.

(a)

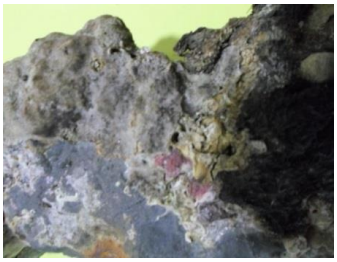

(b)

Figure 8. (a) Subsurface of red oxides under loss part in the external layer from marine sediments that attributed to organic materials; (b) Coloured stains resulting from the bio-activation reactions with iron object. No tests were performed on stains for investigation the bio-corrosion.

(a)

(b)

Figure 9. (a) The interior surface that consists of iron oxy-hydroxide pad under the marine concretion, (b) Active corrosion accuses of weeping aspect due to contaminate with chloride subsequent akaganeite formation with magnetite on top of the iron object.

Destabilization of wrought iron caused by absorption of soluble salts. Drying out the objects without prior treatment leaded to crystallize the salts and destroy the object. So immediate restoration is the best solution for protection the marine objects.

Weeping is attributed to the hygroscopic nature of iron chloride salts whether iron (II, III) chlorides are both hygroscopic [26]. Active corrosion on iron takes the form of shiny, often pustules, wet bubbles of ferrous chloride ('weeping iron'). Weeping iron indicates very unstable iron objects which needs the immediate attention of a conservator as well as a sealed dry storage environment [45].

To prevent further corrosion of iron objects after recovering from saltwater sites, they should be preserved in seawater initially, if no fresh water is available or by keeping the objects wet at all times. They should not be allowed to dry. If objects are dried out prior treatment, iron can corrode, flakes off, and salt contamination becomes difficult to remove [46].

3. Samples preparation for examination and analyses

Two marine iron objects were selected for this study. Small rusted sample were collected by detaching from several different areas using scalpel. For Raman analysis specimens were cut from the objects without preparations where for X-ray diffraction. Samples were not embedded in a resin or dissolution in any solution as acids. All measurements of investigation and analysis were made at room temperature that can change dramatically in chemical structure during the observation.

4. Methodology

Investigation and analysis techniques are the first of conservation steps. They should be performed to determine the corrosion forms and corrosion compounds. Some tests and investigation methods were used prior to performing analyses by Raman as the following. The pH of the oxidized surface was measured by preparation half gram of iron powder that was scraped by using a scalpel blade and mixed with 2mL of distilled water. The mixture was left to equilibrate for 20 minutes. pH measurement was repeated on three separate iron oxidized samples and gave value of 4.5. That means the iron oxides are acidic even though sinking in high alkaline environment.

4.1. Raman spectroscopy

The purpose of the characterization by this method is to obtain spectral signatures for iron corrosion products and marine sediments. Iron corrosion products differ in composition, in the valence of Fe and in crystal structure [47, 48] that forms and colours.

The basis of corrosion identification by Raman spectroscopy is the comparison between the spectra of an unknown material and reference [49]. Raman mapping is not to blame for direct Raman imaging where a large area of the sample is probed all at once. More precisely, only photons from a narrow spectral domain are sent to the CCD detector and each pixel receives those

coming from a given area of the sample [43]. The use of a large sample spot or lowering the laser power significantly reduces the risk of sample damage [www.perkinelmer.com]. The developments of Raman concern the miniaturization of solid laser sources and the replacement of electronic boxes governing the CCD detector (camera) by software, leading to portable Raman instruments. The interaction with electronic levels is anymore virtual because the sample colour and its absorption of the laser light by electronic level. The Raman intensity concentrates in some modes, a small wave number shift is observed and harmonic/combination second order peaks become visible [35].

Archaeological materials are heterogeneous samples that will give non-reproducible results if the spot size of the excitation laser is smaller than the heterogeneous components.

Raman measurements were undertaken using Dispersive Microscope made by Bruker Company (model Senterra spectrometer). Large spot of the sample and lowering power of laser gives high energy without burning the spot area.

The composition and organization of the rust layer must be finely documented to precise the corrosion mechanisms and further obtain some indexes to identify the corrosion products. Three Raman spectra of iron corrosion products were collected at different areas of the first object, and five spectra were collected of the second object.

4.2. Microscopic examination

Examination by Raman microscopy revealed corrosion compounds and crystals of iron objects. Iron corrosion compounds were identified by colours. Illumination and detection was carried out through microscope objective of 20X magnification (constant magnification).

Figure 10a shows the crystallographic nature of iron corrosion products that have spherical form. Intergranular corrosion is the main corrosion form that appears on this area. Goethite and lepedocrocite are the main corrosion products that cover the surface and control the morphological structure. The rust consists of a central red deposit surrounded with other rusted corrosion minerals.

Figure 10b reveals that magnetite is closed with metallic iron and it appears the amorphous structure of iron rust confined between two layers from the metallic iron.

Figure 10c explains different active corroded areas by formation akaganeite that correspond light red rust as unusual part. Also, goethite and lepidocrocite are identified in this area that are covered the most of the sample surface. Rust spots compacted with metallic iron.

Figure 10d shows goethite and lepidocrocite that are the major iron oxides in the outer layer and they would be found around brown to concretionary masses. Iron granular has not geometrical form that is marked out by corrosion compounds.

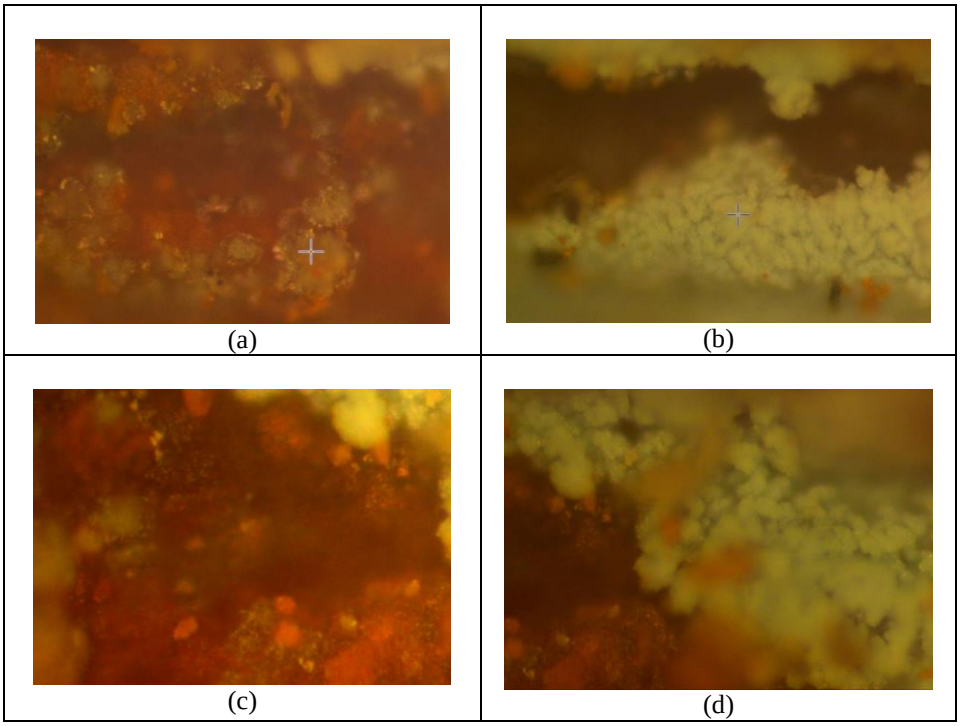

Figure 10. Raman spectroscopy images on cross section of the first marine iron object.

Figure 11a shows iron rust that consists of akaganeite, goethite and lepidocrocite. Akaganeite spreads at different areas and long distance between crystalline and amorphous structure represents corrosion products resulting from the post-excavation corrosion.

Figure 11b seeks to elucidate corrosion minerals that parallel to the metal surface of weathering iron object. Different expansion routes were observed between the longitudinal grains.

Figure 11c shows the iron surface was made up of blackish magnetite with akaganeite in ochre stains.

Figure11d shows the object surface feature that revealed pitting corrosion with porous finish after exposing to seawater for long time. Akaganeite is tightly adhered to the object surface.

Figure 11e shows activation corrosion area from akaganeite with goethite infested this object. Black oxide corresponds to magnetite that represents main corrosion rust appearing in three colours (yellow, red and black).

From the Figures 11a and 11b, layered corrosion is the main corrosion form exhibiting in longitudinal structure as fibres. This phenomenon is called fibrin corrosion. Each grain comprises individually. Grains seen as fibres in longitudinal view distinguish marine wrought iron.

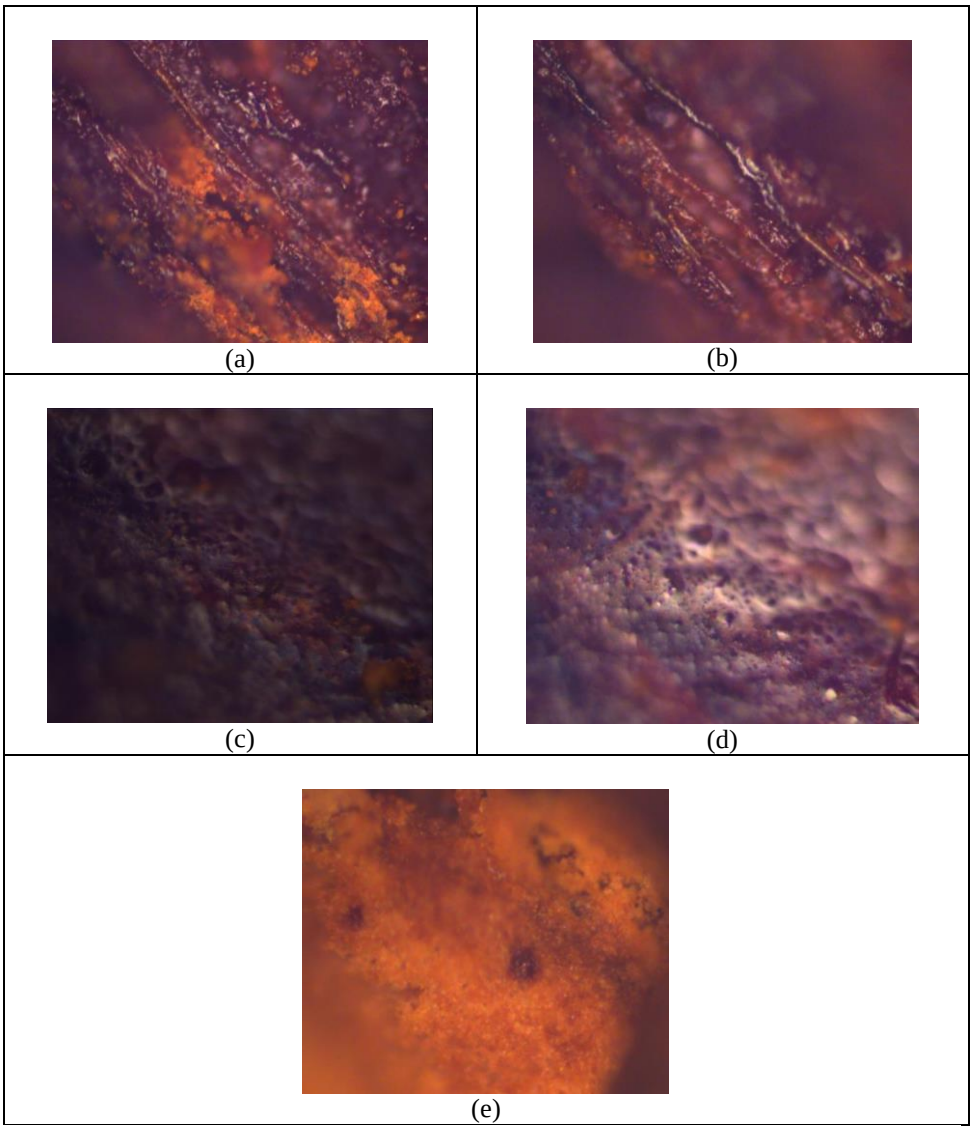

Figure 11. Raman spectroscopy images of the second marine iron object.

4.3. Raman spectra analysis results

As the spectrum of the first object concerns, given in Figure 12a, there is crowding of bands in the 117-1027 cm^{-1} region caused by different iron corrosion products bands, but peaks are not observed in 1028-3176cm^{-1}.

About the second object, there is crowding of bands in the 101-710cm^{-1} region caused by a variety of corrosion products and marine sediments, but peaks are not observed in 710-2773cm^{-1} (Figure 12b).

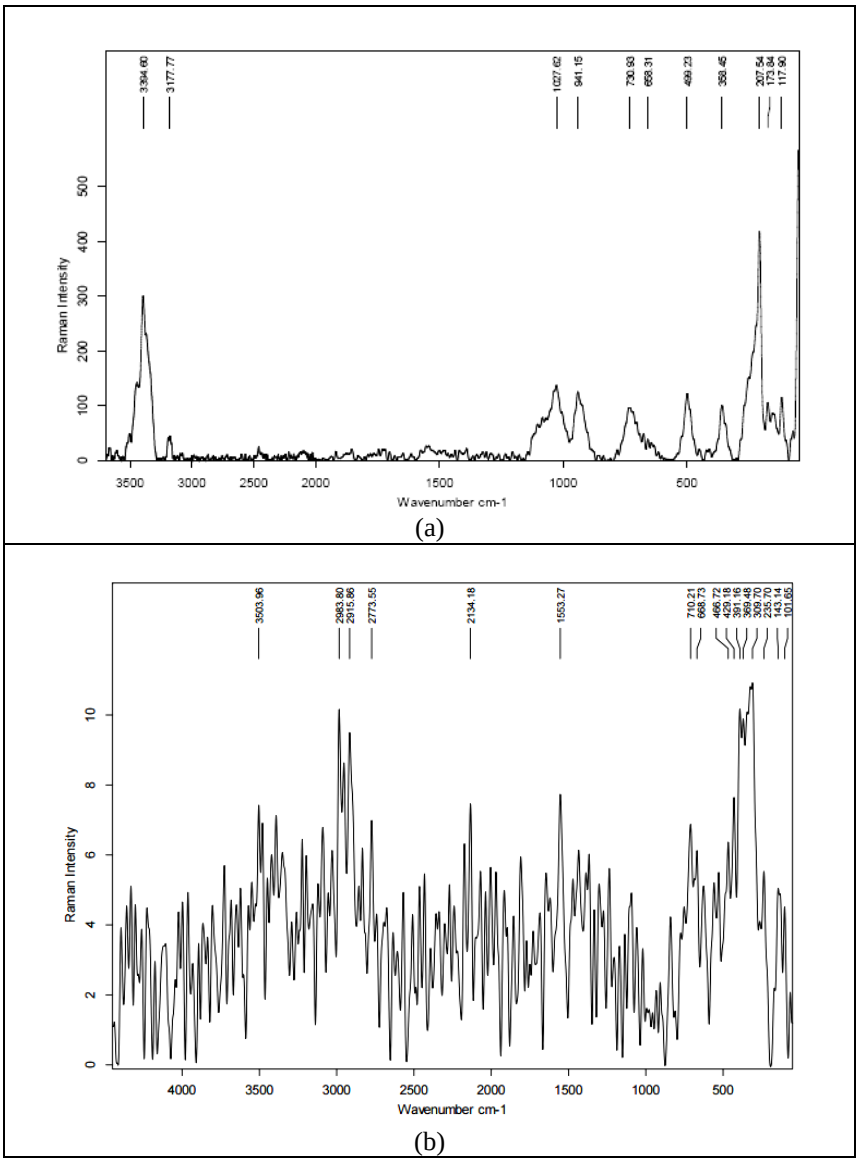

Figure 12. Raman shift of the marine iron corrosion compounds: (a) for the first object; (b) for the second object. The peak shift was presented without smoothing.

4.3.1. Wustite (FeO)

Wustite is the most iron-rich oxide, forming adjacent to the metal [50] that it is a complex nonstoichiometric oxide [51]. Wustite represents the inner layer of corrosion and it is one of the most iron corrosion products [B. Santos, E. Loginova, A. Mascaraque, A. Schmid, K. McCarty and J. Figuera, *Structure and Magnetism in Ultrathin Iron Oxides Characterized by Low Energy Electron Microscopy*, https://arxiv.org/ftp/arxiv/papers/0812/0812.5049.pdf]. The

attained Raman spectrum of wustite is similar in the two objects and it is identified at 688cm^{-1}.This result is in agreement with Suffren [40].

4.3.2. Akaganeite (β-FeOOH)

Akaganeite is the most dangerous corrosion compound, because it is hygroscopic and transforms to other minerals by oxidation. This is an important aspect of its role in post-excavation corrosion. The destructive effect of akaganeite lies on its potential and the conditions of seawater [29]. Chloride ions can be implanted into the tunnels of the crystal lattice of akaganéite (β-FeOOH) [8], which can lead to complete loss of the artefact [9]. For the first object, akaganeite has the bands at 499.23 and 730.93 cm^{-1}, but it has band at 143, 309 and 391 cm^{-1} for the second object. The band values are different between the two objects due to fluorescence background of impurities with the sample.

4.3.3. $Fe(OH)_2$

This compound is formed in a green colour, and it is deposited as a protective film at pH higher than 6 and has minimum solubility at pH 11. It is easily oxidizable and forms intermediate Fe (II, III) compounds (magnetite and green rust). FeOOH compounds are one order of magnitude less soluble than $Fe(OH)_2$ [8]. $Fe(OH)_2$ is not present in the first object, but it was identified in the second object at 466cm^{-1}.

4.3.4. Lepidocrocite (γ-FeOOH)

Lepidocrocite is commonly formed in the early stages of corrosion, and the exposure time increases transformation into goethite [52]. It is produced under the action of oxygen which can subsequently form and consume magnetite [53]. γ-FeOOH is a common terrestrial iron corrosion product which is rarely found on corroded marine iron which reacts with ferrous ion to form magnetite [54]. Lepidocrocite is identified on the basis of the three peaks at 207, 358 and 499 cm^{-1} as observed in the first object. About the second object, Lepidocrocite was detected by characteristic bands at 39 and 369 cm^{-1}.

4.3.5. Goethite (α-FeOOH)

It is an amorphous mineral and a common iron corrosion product [42]. The iron oxyhydroxide (goethite) is formed when a major assertion is that in the oxidized environment [54]. It is a thermodynamically stable compound which shows good protective properties on the iron surface, especially if it is in the form of small particles [8]. Representative bands at 245, 299, 385, 479 and 550 cm^{-1} correspond to a mixture of lepidocrocite and goethite. The Raman

spectrum of goethite shows narrow peaks at 207 and 499 cm^{-1} for the first object, but in the second object shows bands at 235, 309 and 391cm^{-1}.

4.3.6. Feroxyhite (δ-FeOOH)

Iron rust consists essentially of hydrated ferric oxide [55]. The structure of feroxyhite is related to the ferromagnetic δ-FeOOH [56]. It is readily formed by combing any soluble form of Fe^{3+} with hydroxide ions [57]. The presence of feroxyhite was confirmed by its characteristic bands at 499 and 668 cm^{-1} in the first object. About the second object, Feroxyhite was detected from bands at 391 and 668 cm^{-1}.

4.3.7. Schwertmannite (Iron Oxysulfate) $Fe_8^{3+}O_8(OH)_{4.5}(SO_4)O_{1.75}$

A sulphate bearing analogue of akaganéite, is encountered as an early-stage weathering product [http://www.reefkeeping.com/issues/2004-11/rhf/index.php]. One band is obtained for Schwertmannite at 358 cm^{-1} for the first object. The second object does not contain this compound.

4.3.8. Ferrihydrite ($Fe^{3+}{}_5HO_8.9H_2O$) or Fe^{III} oxyhydroxide

It is a generic term which is used to name materials with various degrees of crystallinity [57]. Iron (III) hydroxide is amorphous but over time it is transformed into a crystalline form of iron oxy-hydroxide [8]. At pH 3-14, ferrihydrate is dissolved and redeposited for transformation into goethite [58]. Ferrihydrite has one band in the 730 cm^{-1} region of the first object and in the 391 and 710 cm^{-1} regions for the second.

4.3.9. Iron hydroxychloride (β-Fe(OH)Cl)

The structure of the Fe(II)Fe(III) hydroxychloride (green rust I) precursor stage of these compound becomes unstable when approximately 55% of the total Fe becomes oxidized and the green rust then transforms topotactically by either dehydration and further oxidation to magnetite or by complete oxidation to lepidocrocite [59]. The first object contains iron hydroxychloride that is identified by the peak at 117 cm^{-1}. It was identified at 429 cm^{-1} in the second object.

4.3.10. Magnetite ($FeO{\cdot}Fe_2O_3$)

Magnetite (black rust) is an electronically conducting mixed Fe(II) and Fe(III) iron oxide [26]. It has protective properties due to its thermodynamic stability [8] and it is a common corrosion product identified on archaeological iron excavated from the marine environment. Magnetite has large bands which may be assigned phases by dimensional effects or pressure on the microcrystals

[60]. Green hydrated magnetite $Fe_3O_4 \cdot H_2O$ can occur in seawater [61]. Oxidation of magnetite by further laser heating leads to hematite [62]. It seems for the first object to assign the Raman band at 499, 668, 730 and 1027 cm^{-1}. About the second object, it is obvious that this compound was detected at 668 and 710 cm^{-1}.

4.3.11. Maghemite (Fe_2O_3)

Maghemite has a similar crystalline structure to magnetite and the same chemical composition as hematite [63]. In cases where magnetic measurements cannot distinguish between magnetite and maghemite, because they are ferromagnetic oxides, therefore Raman spectra are the best method that can be used for identification [64]. From the Raman shift peaks, maghemite is identified at 358, 499, 668 and 730 cm^{-1} for the first object. Also, Raman shift showing characteristic peaks at 369, 668, 710 and 1553 cm^{-1} for the second object.

4.3.12. Hematite (Ferric oxide α-Fe_2O_3)

Hematite is the most stable and widespread oxide phase of iron [47]. On the Raman spectrum of hematite, the presence of a peak at about 660 cm^{-1} has been neglected, even though it is present in several published spectra [60]. The red oxides showed Raman spectra with bands of hematite at 207 and 499 cm^{-1} for the first object and at 235, 309 and 391 cm^{-1} for the second object.

4.3.13. Siderite ($FeCO_3$)

Siderite is one of the rust compounds that result from reaction of dissolved carbon dioxide with iron. Siderite bands are easy to obtain as the mineral is stable at moderate laser power [51]. For the first object, Siderite is characterized by the peak at 730 cm^{-1}, but it was not detected in the second object.

4.3.14. White rust

White rust is a localized corrosion that consists of pure hydroxides, carbonates and sulphates [65]. White rust is a complex, hydrated zinc carbonate/zinc hydroxide. The Raman spectrum of white rust for the first object indicated that it corresponds to representative bands at 1027 cm^{-1}. For the second object, the peak at 369 cm^{-1} is attributed to white rust.

4.3.15. Minium

Minium might be resulted from impurities with iron that has a weak band at 117 cm^{-1} for the first object, but it is not identified in the second object sample.

Table 1. List of the marine iron corrosion products associated with the wrought iron objects, their characteristic Raman fingerprints and their standard references. Indicators 'V.S' (very strong), 'S' (strong), 'M' (moderate) and 'W' (weak) refer to band intensity.

Compounds	Formula	Characteristic wavelength (cm^{-1})		Published values	Ref.
		1st objects	2ndobject		
Wustite	FeO	668(M)	668.73(M)	595-616-655-663-663	[40]
Akaganeite	β-FeOOH	499.23(M)-730.93(W)	143.14(M)-309.70(V.S)-391.16(M)	140-300-309-310-311-314-380-390-395-415-497-541-549-720-722-723-725-745	[25, 40, 62, 66, 68, 69, 70]
Lepidococite	γ-FeOOH	207(M)-358.45(M)-499(M)	309.70(V.S)-369.48(S)	216-217-219-245-250-251-252-309-311-347-348-349-350-375-378-380-493 -499-527-648-650-651-655-1300-1302-1307	[25, 42, 65, 69, 70, 71, 72]
Goethite	α-FeOOH	207.54(V.S)-499.23(M)	235.70(M)-309.70(V.S)-391.16(M)	163-202-205-244-247-299-300-388- 390-400-418-481-498-500-550-553 -1003-1086	[25, 65, 69, 70, 72, 73]
Ferroxyhite	δ-FeOOH	668.31(M)	391.48(M)-668(M)	297-330-392-400-650-663-666-666-668-680-1322-1350	[65, 69, 72]
Schwertmannite	$Fe_8^{3+}O_8(OH)_{4.5}(SO_4)O_{1.75}$	358(M)	----------	350	[65]
Ferrihydrites	$Fe_5HO_8{,}4H_2O$	730.93(W)	391.48(M)-710.21(M)	390-710-725-510-1315-1380	[34, 65, 71]
Iron chloride	$FeCl_2$	---------	--------	610	[65]
Iron hydroxychloride	β-$Fe_2(OH)_3Cl$	117.84(M)	429.18(W)	127-160-423	[65, 68]
Magnetite	Fe_3O_4	499(M)-668.31(M)-730.93(W)-1027(M)	309-668.73(M)-710.21(M)	298-319-490-507-532-535-540-663.6-658-662-663-665-667-667-668-668-670-671-671-673-700-722-1020	[25, 34, 62, 64, 65, 68, 69, 72]
Maghemite	γ-Fe_2O_3	358.45(M)-499(M)-668.31(M)-730.93 (W)	369.48(S)-391.48-668.73(M)-710.21(M)-1553.27(S)	344-350-360- 360-377-381-390-499-500-510-670 - 665-668-668-670-715-720-721-730-1320-1400-1560	[62, 64, 65, 69, 71, 72]
Hematite	α-Fe_2O_3	207(V.S)-499.23(M)	235.70(M)-309.70(V.S)-391.16(M)-668.73	210-219-220-223-225-226-247-285-286-289-290-293-300-396-405-412-497-498-499.1-500-501-613-668-1306-1310-1316	[60, 62, 64, 65, 69, 71, 72, 74]
Siderite	$FeCO_3$	730.93(W)	----------	731	[65]
Mackinawite	FeS	207(V.S)	309.70 (V.S)	180-200-209-212-253-257-280-283-296-298-300	[62, 65]
Pyrite	FeS_2	--------	369.48(S)	345-370	[*]
Greigite	Fe_3S_4	358.45(M)	--------	350-360	[65]
	$Fe(OH)_2$	---------	466.72(W)	460- 550	[72]
Fyalite	Fe_2SiO_4	358-499(M)	---------	356-405-505-580	[75]
Iron hydroxide	$Fe(OH)_3$	---------	391.16(M)	395-692- 696- 1335	[72]
Green rust		------	429.18(W)	430-510	[65]
White rust	$3Zn(OH)_2 \cdot 2Zn_3$	1027.62(M)	369.48(S)	370-1020- 1050	[34]
Minium	$Pb^{2+}\ 2Pb^{4+}O_4$	117.9(M)	----------	120	[65]
Quartz	α·SiO_2	207.54(V.S)-358.54(M)	---------	148-205-357	[60, *, 76]
Gypsum	$CaSO_4 \cdot 2H_2O$	1027(M)-3394.60(S)	--------	140-415-1007-1132-3400	[70, 72, 77]
Orthoclase	$KAlSi_3O_8$	499.23(M)	---------	500	[74]

[*] - http://www.fis.unipr.it/phevix/ramandb.html

4.3.16. Greigite (Fe_3S_4)

Greigite is strongly magnetic responding like magnetite [66] that can be produced by bacteria [67]. The spectrum consists of broad, weak and narrow band at 358 cm^{-1} for the first object, but it is not identified in the second object.

4.3.17. Gypsum

Gypsum crystals associated with weathered iron covers the metallic iron core gradually and control in corrosion rate. Raman spectrum of gypsum is 1027 and 3394 cm^{-1} for the first object, but it is not identified in the second object.

4.3.18. Quartz and Orthoclase

These minerals resulted from marine encrustations. Quartz is clearly visible at bands 207 and 358 cm^{-1}.The peak at 499 cm^{-1} is allocated to orthoclase, but they are not identified in the second object. The results of Raman spectroscopy analyses are summarized in Table 1.

Characteristic wavelength of corrosion products was identified by comparison to the standard reference and other values from literature assignment that is found in the column of published values. Collection data of reference phases and their spectra values were obtained to identify the corrosion products. Samples from the first object, three peaks at 941, 3177 and 3394 cm^{-1} and six peaks at 101, 2134, 2773, 2915, 2983 and 3503 cm^{-1} for the second object are detected but they are not reported in the literatures of iron corrosion compounds. The bands value look like in the two objects just at 688 cm^{-1} that corresponds of magnetite, maghemite, wustite and ferroxyhite. For the first object, magnetite and maghemite have the same peaks, just at 358cm^{-1} (maghemite) and 1027 cm^{-1} (magnetite). About the second object, the difference between magnetite and maghemite at 396 and 1553 cm^{-1} that corresponds of maghemite.

The results were checked by X-ray powder diffraction analysis for proving Raman spectra results, but this technique has limitation for distinction between corrosion compounds as maghemite γ-Fe_2O_3 and magnetite Fe_3O_4 which they have the same diffraction pattern.

Table 2. X-ray powder diffraction analysis results of iron corrosion products. Indicators ‘V.S’ (very strong), ‘S’ (strong), ‘M’ (moderate).

Minerals	**Mag.**	**Aka.**	**Magh.**	**Hem.**	**Geo.**	**Lep**	**Orth.**	**Quar.**
Ratio	**V.S**	**S**	**M**	**W**	**M**	**M**	**M**	**M**

Table 2 shows the corrosion products that were identified by X-ray diffractometry. The difference between XRD patterns and Raman spectra is concentrated in the ratio. Also, magnetite and akaganeite are the major of corrosion products in the first object.

After identification of corrosion products, they should be removed or reduced before preservation process.

5. Conclusions

This work deals with the mechanisms of corrosion process of wrought iron objects removed from saline water that corresponds with an unstable environment. Wrought iron objects were mostly transformed in to corrosion products resulting from their activity to corrosion process and exposure to continuous changes in saline water. Photo-documentation over times showed visual changes by further corrosion. It is clear that Raman method is an important method for identifying the corrosion products of metallic artefacts, and assesses the condition of marine iron objects, because it is a rapid, an inexpensive, non-destructive and accurate method for investigation and analysis. Iron oxides strongly absorb laser light, hence Raman spectroscopy was performed to characterize corrosion products and marine sediments. Raman spectra are based on the concentration of iron corrosion products exhibited to seawater which concluded heavily corrosion rate, caused by the effect of chloride ions. Imaging by microscopic investigation describes the assignment of various corrosion phases and the features associated with different iron corrosion products.

Also, Raman spectroscopy is a technique that was performed to determined physical structure by microscopic investigation of corrosion products that have characteristics forms than other methods. Raman spectra results proved that the identified iron corrosion products were typically found in the literature review.

The peak distributions are not the same for the two iron objects because their chemical structures are not similar. The bands value look like in the two objects just at 688 cm^{-1} that corresponds of magnetite, maghemite, wustite and ferroxyhite.

Goethite, hematite, lepidocrocite and akaganeite are the major corrosion products that they are highly detected in the rust and these results agree with most of previous literature. Also, Raman spectroscopy indicated the presence of iron oxide and oxy-hydroxide in the two objects. Raman spectroscopy shows that as the concentration of magnetite increases, the concentration of akaganeite decreases resulting from destroying the protected layer of magnetite. There are difference in the peaks between Magnetite and maghemite.

The difference between our results of spectra and standard reference is due to fluorescence background of impurities with the sample. The two iron objects are not completely transformed into corrosion compounds, which it can be conserved by reduction methods as electrical or plasma reduction.

Acknowledgement

The cooperation of Peter Nicolaides (Oceanographer) and his team work at Aegean Institute, Greece is gratefully acknowledged regarding leaching of the metal objects from Paros Island. I thank Dr. Amr Nabeel, researcher at Egyptian Petroleum Research Institute, for his assistance in the analysis of some iron samples. Special thanks are due to Dr. Ahmed Lotfy, Helwan University, for the great efforts of editing this paper.

References

[1] F. Laque, *Marine corrosion, causes and preservation*, John Wiley and Sons, New York, 1975, 7.
[2] N. North, Stud. Conserv., **27** (1982) 76-83.
[3] M. Gilberg and N. Seeley, Stud. Conserv., **26** (1981) 50-56.
[4] J. Argo, Stud. Conserv., **26** (1981) 42-44.
[5] H. Steyne, and I. Macleod, Bulletin of the Australasian Institute for Maritime Archaeology, **35** (2011) 67-80.
[6] D. Watkinson and M. Lewis, Stud. Conserv., **50** (2005) 241-252.
[7] D. Shifler and D. Aylorm, *Seawater, Corrosion Tests and Standards: Application and Interpretation*, R. Babian (ed.), ASTM, USA, 2005, 362.
[8] B. Polić-Radovanović Jegdić, S. Ristić and S. Alil, Scientific Technical Review, **61(2)** (2011) 50-56.
[9] C. Degrigny, D. Vella and S. Golfomitsou, J. Crawford, *Characterisation of Corrosion Product Layers on Atmospherically Corroded Ferrous Artefacts: Application to the Armour of Armoury Palace, Valletta, Malta*, Proc. of International Conference on Conservation Strategies for Saving Indoor Metallic Collections with a Satellite Meeting on Legal Issues in the Conservation of Cultural Heritage, TEI, Athens, 2007, 31-39.
[10] S. Durowaye, A. Alabi, O. Sekunowo, B. Bolasodun and I. Rufai, International Journal of Engineering and Technology, **4** (2014) 139-143.
[11] M. Clugston and R. Flemming, *Advanced Chemistry*, Oxford University Press, Oxford, 2007, 233.
[12] N. Sato, *Basics of Corrosion Chemistry, Green Corrosion Chemistry and Engineering: Opportunities and Challenges*, S. Sharma (ed.), Wiley-VCH Verlag GmbH & Co. KGaA, Weinheim, 2012, 1-16.
[13] C. Arnaud, Chem. Eng. News, **85(2)** (2015) 45-47.
[14] C. Vargel, *Corrosion of Aluminum*, Elsevier, Oxford, 2004, 335-336.
[15] P. Roberge, *Handbook of Corrosion Engineering*, McGraw-Hill, New York, 1999, 14.
[16] M. Heldtberg, I. MacLeod and V. Richards, *Corrosion and Cathodic Protection of Iron in Seawater: A Case Study of the James Matthews (1841)*, Proc. of Metal 2004, National Museum of Australia, Canberra, 2004, 75-87.
[17] D. Hamilton, Archives and Museum Informatics, **13** (2001) 291-322.
[18] H. Lowenstam, *Impact of Life on Chemical and Physical Process*, in *Marine Chemistry Science*, E. Goldberg (ed.), Harvard University Press, London, 2005, 745.
[19] W. Rahmanto and R. Nuryanto, Journal of Coastal Development, **5** (2002) 68-74.
[20] S. Paul, ISRN Metallurgy, **2012** (2012) 1-6.

[21] B. Hasan, College of Engineering Journal, **13** (2010) 66-73.
[22] H. Weinreben, S. Wolf, P. Seitz, B. Spitzer, G. Adel, B. Nausch and D. Wright, Ocean Science, **6** (2010) 4-24.
[23] G. Tompson and J. Turk, *Earth Science and The Environment*, Saunders College Publishing, New York, 1993, 347.
[24] M. Mladen, *Causes of the Decay of Archaeological Material*, in *Conservation of Underwater Archaeological Finds Manual*, B. Luka (ed.), International Centre for Underwater Archaeology, Zadar, 2011, 19-20.
[25] M. Veneranda, J. Aramendia, O. Gomez, S. Vallejuelo, L. Garcia, I. Garcia-Camino, K. Castro, A. Azkaratec and J. Madariaga, J. Raman Spectrosc., **48** (2016) 258-266.
[26] L. Selwyn, *Overview of archaeological iron: the corrosion problem, Key Factors Affecting Treatment, and Gaps in* Current knowledge, Proc. of Metal 2004, National Museum of Australia, Canberra, 2004, 295-306.
[27] D. Watkinson, *Preservation of Metallic Cultural Heritage*, in *Shreir's Corrosion*, R.A. Cottis (ed.), 4th edn., Vol. 4, Elsevier B.V., London, 2010, 3307-3340.
[28] A. Oluwaseun and I. Simeon, Journal of Chemical Engineering and Materials Science, **6** (2015) 52-57.
[29] M. Rimmer, *Investigating the treatment of chloride-infested Archaeological Iron Objects*, PhD Thesis, Cardiff University, Cardiff, 2010, 52.
[30] D. Bayliss and D. Deacon, *Steelwork Corrosion Control: from the Middle Ages to the Renaissance*, 2nd edn., Taylor and Francis, United Kingdom, 2002, 7-305.
[31] S. Loridant, G. Lucazeau and T. Le-Bihan, J. Phys. Chem. Solids, **63(11)** (2002) 1983-1992.
[32] A. Philip and E. Schweitzer, *Encyclopedia of Corrosion Technology*, CRC Press, New York, 2004, 75-232.
[33] S. White, Chem. Geol., **259** (2009) 240-252.
[34] L. Bellot-Gurlet, D. Neff, S. Reguer, J. Monnier, M. Saheb and P. Dillmann, Journal of Nano Research, **8** (2009) 147-156.
[35] P. Colomban and M. Havel, J. Raman Spectrosc., **33** (2002) 789-795.
[36] H. Nalwa, *Silicon-Based Material and Devices, Materials and Processing, Properties and Devices*, Academic Press, London, 2001, XI.
[37] J. Ambers, *Introduction*, in *Raman Spectroscopy in Archaeology and Art History*, H. Edwards & J. Chalmers (eds.), Royal Society of Chemistry, London, 2005, 7.
[38] M. Yadav, *A Textbook of Spectroscopy*, 2ndedn., J. Anmol Kumarr publication Pvt. Ltd., New Delhi, 2003, 326.
[39] R. Baddour-Hadjean and J. Pereira-Ramos, Chem. Rev, **110** (2010) 1278-1291.
[40] Y. Suffren, F. Rollet and C. Reber, *Raman Spectroscopy of Transition Metal Complexes: Molecular Vibrational Frequencies, Phase Transitions, Isomers, and Electronic Structure*, Taylor & Francis Group, London, 2011, 248-254.
[41] K. Lee and T. Herrman, C. Nansen and U. Yun, International Journal of Regulatory Science, **1** (2013) 1-14.
[42] P. Montoya, T. Marín, A. Echavarría and J. Calderón, Int. J. Electrochem. Sc., **8** (2013) 12566-12579.
[43] G. Gouadec and P. Colomban, Prog. Cryst. Growth Ch., **53(1)** (2007) 1-56.
[44] I. Macleod, Bulletin of the Australian Institute for Maritime Archaeology, **13(2)** (1989) 7-16.
[45] K.R. Singley, OAHP, (2014) 1536.
[46] D. Riss, Conserve O Gram, **6(1)** (1993) 1.

[47] G. Schmid, *Nanoparticles from Theory to Application*, 2nd edn., Wiley-VCH: Weinheim, 2010, 522.
[48] M. Iacob, Chemistry Journal of Moldova General, Industrial and Ecological Chemistry, **10** (2015) 46-51.
[49] W. Griffith, *Advances in the Raman and Infrared Spectroscopy of Minerals*, in *Spectroscopy of Inorganic-Based Materials*, R. Clark & R. Hester (eds.), Wiley, New York, 1987, 119.
[50] V. Fell, *Cremated: Analysis of the metalwork from an Iron Age grave*, Proc. of Metal 2004, National Museum of Australia, Canberra, 2004, 512-519.
[51] R. Hazen and R. Jeanloz, Rev. Geophys., **22** (1984) 37-46.
[52] R. Antunes, I. Costa and D. Araújo de Fari, J. Mat. Res., **6** (2003) 403-408.
[53] T. Skerry, J. Bitensky and E. Lanyon, J. Orthopaed. Res., **6** (1988) 547-551.
[54] R. Mark and J. Nigel, Stud. Conserv., **26** (1981) 50-56.
[55] D. Nev, *Apport des Analogues Archéologiques à l'estimation des Vitesses Moyennes et à l'étude des Mécanismes de Corrosion à Très Long Terme des Aciers non Alliés Dans les Sols, Sciences Mécaniques pour l'lngénieur*, Université de Technologie de Compiègne, Compiègne, 2000, 360.
[56] J. Hederson, *Metallurgy Dictionary*, Reinhold Publishing Corporation, New York, 1953, 92.
[57] L. Carlson and U. Schwertmann, Clay. Clay Miner., **28** (1980) 272-282.
[58] T. Pedersen, Meteorit. Planet. Sci., **34** (1999) 143-149.
[59] R. Bolanz, J. Majzlan, U. Bläss, V. Ciobota, S. Ackermann, L. Palatinus, T. Reich and M. Kersten, *The Transformation of Ferrihydrite into Goethite, Hematite and Feroxyhyte in The Presence of Sb(V), As(V), and P(V)*, Jena School for Microbial Communication, Jena, 2011, 1-16.
[60] R. Taylor, Clay. Clay Miner., **32** (1984) 75-180.
[61] D. Bersani, P. Lottici and A. Montenero, J. Raman Spectrosc., **30** (1999) 355-360.
[62] D. Hamilton, Methods for Conserving Archaeological Material from Underwater Sites, Texas A&M University, Washington, 1999, 56.
[63] G. Gencheva and A. Erbe, J. Electrochem. Soc., **163** (2016) C334-C338.
[64] M. Chirita and I. Grozescu, Chem. Bull. 'Politehnica' Univ. Timisoara, **54** (2009) 1- 2.
[65] M. Hanesch, Geophys. J. Int., **177** (2009) 941- 946.
[66] P. Colomban, *Potential and Drawbacks of Raman (Micro) Spectrometry for the Understanding of Iron and Steel Corrosion*, in *New Trends and Developments in Automotive System Engineering*, M. Chiaberge (eds.), Intech Europe, Rijeka, 2011 570.
[67] B. Skinner, R. Erd, F. Grimaldi and F. Greigite, Journal of The Mineralogical Society of America, **54** (1964) 326-330.
[68] J. Wang, S. Cao, W. Wu and G. Zhao, Phys. Scr., **83** (2011) 1-5.
[69] D. Neff, S. Reguer, L. Bellot-Gurlet, P. Dillmann and R. Bertholon, J. Raman Spectrosc., **35** (2004) 739-745.
[70] A. Legodi, *Raman Spectroscopy Applied to Iron Oxide Pigments from Waste Materials and Earthenware Archaeological Objects*, PhD Thesis, University of Pretoria, Pretoria, 2008, 70.
[71] D. Bersani, P. Lottici and A. Casoli, *Case study: Microraman and GC-MS of Frescoes*, in *Raman Spectroscopy in Archaeology and Art History*, Royal Society of Chemistry, Cambridge, 2005, 187–228.
[72] L. Mazzetti and P. Thistlethwaite, J. Raman Spectrosc., **33** (2002) 104-111.
[73] J. Sei, D. Cook and H. Townsend, Hyperfine Interact., **112** (1998) 59-65.

[74] S. Scardova, P. Lottici, D. Bersani, G. Antonioli, G. Michiara and C. Pezzani, Stud. Conserv., 47 (2002) 24-28.
[75] K. Gussem, P. Vandenabeele and L. Moens, J. Raman Spectrosc., **38** (2007) 1133-1147.
[76] A. Cnopnras, Am. Mineral., **76** (1991) 1105-1109.
[77] I. Groot, H. Ankersmit, R. Langh and W. Wei, *Corrosion layers on historic iron artifacts*, Proc. of Metal 2004, National Museum of Australia, Canberra, 2004, 309-313.
[78] Y. Wang and F. Meldrum, J. Mater. Chem., **22** (2012) 22055-22062.